Ocean Engineering 179 (2019) 67–75

Contents lists available at ScienceDirect

Ocean Engineering

journal homepage: www.elsevier.com/locate/oceaneng

Experimental and numerical investigations of advancing speed effects on hydrodynamic derivatives in MMG model, part I: X_{vv},Y_v,N_v

Chenliang Zhang[a,b], Xiaojian Liu[b], Decheng Wan[a], Jinbao Wang[b,*]

[a] State Key Laboratory of Ocean Engineering, School of Naval Architecture, Ocean & Civil Engineering, Shanghai Jiao Tong University, Shanghai, China
[b] Shanghai Key Laboratory of Ship Engineering, Marine Design and Research Institute of China, Shanghai, China

ARTICLE INFO

Keywords:
ONR Tumblehome
Oblique towing
Hydrodynamic derivatives
Advancing speed
MMG model

ABSTRACT

Experimental and numerical studies on the hydrodynamic forces and moments of the ONR Tumblehome (ONRT) hull during oblique towing tests are performed. The experiments are carried out in the towing tank of Marine Design and Research Institute of China (MARIC) and the numerical simulations are based on the open-source CFD library OpenFOAM. Validations of the numerical methods are provided by comparison with experimental measurements from tests at two advancing speed. And then the investigations of advancing speed effects on hydrodynamic derivatives used in MMG model are performed numerically. Specifically, X_{vv}, Y_v, N_v of the ONRT hull at four advancing speed are yielded via linear regression of the hydrodynamic forces and moments predicted by CFD calculations. Finally, the relationship between hydrodynamic derivatives and advancing speed are concluded and the expressions of hydrodynamic derivatives that can be used in MMG model are given.

1. Introduction

Ship maneuverability is the ability of a ship to keep or change its state of motion under the operations of rudder and propeller, which plays a critical role in relation to navigation safety and economy of a ship. It includes inherent dynamic stability, course keeping stability, initial turning ability, yaw checking ability, turning ability and stopping ability. To evaluate ship maneuverability, the "Standards for Ship Maneuverability" were proposed by the IMO (International Maritime Organization) and various kind of standard maneuvers, such as turning test, zig-zag test, stopping test, pull-out test et al., were proposed to yield significant quantities.

According to the IMO "Standards for Ship Maneuverability", maneuvering performance of a ship should be designed to comply with the standards at the design stage. Therefore, the prediction of the ship maneuvering performance should be conducted at the early design stage. Generally speaking, there are two methods for this purpose, specifically the free-running model tests or the captive model tests together with mathematical models. And with the progress of CFD (computational fluid dynamics) techniques and HPC (high-performance computers), numerical simulations are widely used in the predictions of ship maneuvering (Carrica et al., 2013; Shen et al., 2015; Mofidi and Carrica, 2014; Sadat-Hosseini et al., 2014; Broglia et al., 2015). performed numerical simulations of free-running tests, such as turning and zig-zag tests, of various hull forms and the predicted results are in good agreement with experimental model tests. As for mathematical models, the ship maneuvering motions can be expressed as an ordinary differential equation which is derived according to the Newton second law. In the equation, there are two methods for expression of the external forces and moments acting on the ship. One called Abkowitz model, as is proposed in (Abkowitz, 1964), is based on Taylor-series expansions with the hydrodynamic forces and moments expressed as functions of kinematical parameters and rudder angle. The other one called MMG (Mathematical Modeling Group) model is first introduced in (Ogawa et al., 1977). In this model, the hydrodynamic forces and moments are decomposed into three parts, i.e., the parts acting on the hull, the propeller and the rudder. Compared to Abkowitz model, the main advantage of the MMG model is that, all the hydrodynamic derivatives used in the model have explicit physical meanings which makes it easier for a clear understanding of ship maneuvering motions. The hydrodynamic derivatives used both in the Abkowitz and MMG model can be determined through captive model tests, specifically speaking, the oblique towing tests, circular motion tests and dynamic PMM tests (Mucha and El Moctar, 2015). predicted maneuverability of a mariner, a tanker and a ferry ship using Abkowitz model with the hydrodynamic derivatives yielded from model tests (Sung and Park, 2015; He et al., 2016). performed maneuvering predictions using MMG model based on CFD generated derivatives. As illustrated in the literature, there are

* Corresponding author.
E-mail address: wang_jb@maric.com.cn (J. Wang).

https://doi.org/10.1016/j.oceaneng.2019.03.019
Received 6 November 2018; Received in revised form 8 March 2019; Accepted 11 March 2019

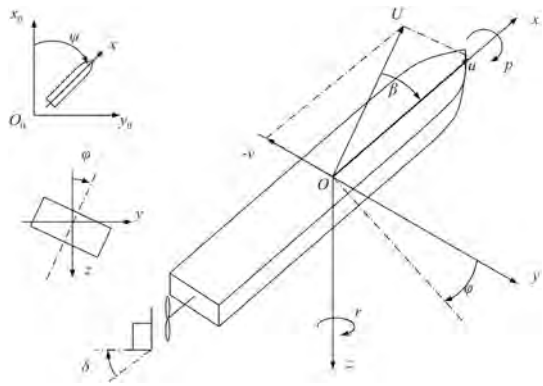

Fig. 1. Coordinate system.

some differences between predictions obtained from mathematical models and free-running model tests, but considering the high efficiency of the mathematical model, it is also widely used in the early design stage of ships. The present work is based on the MMG model and a brief introduction will be given hereinafter.

1.1. MMG model

The MMG model is a simplified mathematical model for solving ship maneuvering problems. It was first proposed in (Ogawa et al., 1977) by a research group called Maneuvering Modeling Group in Japanese Towing Tank Conference (JTTC). To date, considerable simulation methods based on the MMG model for ship maneuvering have been presented. On the purpose of avoiding inadaptability of hydrodynamic derivatives to different modified methods, in (Yasukawa and Yoshimura, 2015), an MMG standard method for ship maneuvering predictions was proposed. The study in this paper was based on this method and a brief introduction of this method will be given in the following text.

Fig. 1 shows the coordinate system used in this article. $O_0 - x_0y_0z_0$ is the earth-fixed coordinate system where x_0y_0 plane coincides with the still water surface and the z_0 axis points downward. $O - xyz$ is the body-fixed coordinate system with the origin O taken at the center of gravity of the ship, and the x, y, z axes point respectively towards the bow, the starboard and downward. $U \equiv \sqrt{u^2 + v^2}$ represents the advancing speed of the ship and u, v denote the velocity components along x, y axes. β denotes the drift angle of the ship and is defined as $\beta \equiv \arctan(-v/u)$. r, p are the yaw rate and roll rate of the ship and ψ, φ denote the heading angle and rolling angle.

As described in (Yasukawa and Yoshimura, 2015), the hydrodynamic forces acting on the ship can be expressed as Eqn. (1).

$$\begin{cases} X = X_H + X_R + X_P \\ Y = Y_H + Y_R + Y_P \\ N = N_H + N_R + N_P \end{cases} \tag{1}$$

where the subscript H, R, P represent hull, rudder and propeller, respectively. In present work, the hydrodynamic forces acting on the bare hull are investigated and it is expressed as Eqn. 2

$$\begin{cases} X_H = -R_0 + X_{vv}v^2 + X_{vr}vr + X_{rr}rr + X_{vvvv}v^4 \\ Y_H = Y_v v + Y_r r + Y_{vvv}v^3 + Y_{vvr}v^2r + Y_{vrr}vr^2 + Y_{rrr}r^3 \\ N_H = N_v v + N_r r + N_{vvv}v^3 + N_{vvr}v^2r + N_{vrr}vr^2 + N_{rrr}r^3 \end{cases} \tag{2}$$

In Eqn. (2), X_{vv}, X_{vr}, X_{rr}, X_{vvvv}, Y_v, Y_r, Y_{vvv}, Y_{vvr}, Y_{vrr}, Y_{rrr}, N_v, N_r, N_{vvv}, N_{vvr}, N_{vrr}, N_{rrr} are hydrodynamic derivatives, where X_{vv}, X_{vvvv}, Y_v, Y_{vvv}, N_v, N_{vvv} are obtained through oblique towing tests and X_{vr}, X_{rr}, Y_r, Y_{vvr}, Y_{vrr}, Y_{rrr}, N_r, N_{vvr}, N_{vrr}, N_{rrr} are obtained through dynamic PMM tests, specifically pure yaw and pure sway tests, or circular motion test. In the present work, we will mainly discuss hydrodynamic forces related to lateral velocity v and both experimental and numerical oblique towing tests were conducted, so that all the hydrodynamic derivatives related to yaw rate r can be eliminated.

As is stated in the introduction, all the hydrodynamic derivatives used in the MMG model have explicit physical meanings. Hydrodynamic derivatives related to lateral velocity v, which are obtained through the oblique towing test, mean the force or moment induced by a unit component of velocity along y axis in maneuvering motions. However, all the hydrodynamic derivatives are deduced at the initial state with a certain value of forwarding speed and will remain constant during maneuvering motions. As is illustrated in (Liu et al., 2017), a significant amount of speed loss occurs during maneuvering motions, like full turning or zig-zag motions, both in free running model tests and sea trials. As a result, it is theoretically inappropriate to treat all the hydrodynamic derivates invariant as used to in the MMG standard model. In (Simonsen and Stern, 2014), the oblique towing tests of the DTMB-5415 hull were performed at 4 different towing speed, but the specific relationship between towing speed and hydrodynamic derivatives was not given.

The purpose of this article is to investigate the effects of advancing speed on hydrodynamic derivatives and yield an expression between them. At small value of lateral velocity v, the relationship between hydrodynamic forces and lateral velocity is roughly linear, so the nonlinear term like X_{vvvv}, Y_{vvv}, N_{vvv} can be neglected and only three linear hydrodynamic derivatives X_{vv}, Y_v, N_v need to be considered. Accordingly, Eqn. (1) can be rewritten as Eqn. (3) in the present work.

$$\begin{cases} X = X_H = -R_0(U) + X_{vv}(U)\cdot v^2 \\ Y = Y_H = Y_v(U)\cdot v \\ N = N_H = N_v(U)\cdot v \end{cases} \tag{3}$$

2. Outline of model tests

2.1. Geometry and general parameters

In this work, the ONR Tumblehome (ONRT) bare hull, which is the 2015 Tokyo CFD workshop benchmark hull form without bilge keels, twin rudders and propellers, is considered. The test model is made of wood and is illustrated in Fig. 2, of which the scale ratio is $\lambda \equiv 1/30$. The general ship parameters are listed in Table 1.

2.2. Experiment setup

The PMM model tests were carried out in Marine Design and Research Intitute of China (MARIC). MARIC's towing tank is 280 m long, 10 m wide and 5 m deep. The maximum speed of the towing carriage is $9m/s$ and the accuracy of towing speed is about 0.1% of the maximum speed. The planar motion mechanism used in the model test is shown in Fig. 2, of which the maximum amplitude of sway and yaw motion are respectively $0.75m$ and 45°. The mechanism is mainly

Fig. 2. Planar motion mechanism.

Table 1
General ship parameters.

Parameter	Design draft	
	Full scale	1/30 Model Scale
Waterline length L_{wl} (m)	154.0	5.133
Beam B (m)	18.78	0.626
Draft d (m)	5.494	0.183
Displacement ∇ (m^3)	8507	0.315
Block Coefficient C_B	0.535	
LCG from aft extent (m)	74.47	2.482
VCG from baseline (m)	7.620	0.250
K_{xx}/B	0.444	
K_{yy}/L_{wl}	0.250	
K_{zz}/L_{wl}	0.250	
Design speed U_0 (m/s)	7.765	1.418

composed of three part, specifically, a computer-controlled transverse system that controls the amplitude and period of sway motion, a rotation module that controls the amplitude and period of yaw motion and a slideway which connects the hull model with force transducers. During the PMM model test, the mechanism carrying the hull model was connected to the towing carriage. The hull model was free to trim and sink, otherwise constrained. The longitudinal force X, transverse force Y and yaw moment N were measured by two 2-component gauges. Two force transducers were symmetrically placed respect to the center of gravity of the hull model with 1.6 m separation. The experimental measurements will also be 2019 SIMMAN Workshop's benchmark data.

In order to ensure the accuracy of the drift angle in oblique towing tests and pure sway, yaw motion amplitude, the planar motion mechanism was calibrated at first. Several drift angles, several periods of pure sway and pure yaw motions were tested before the mechanism was mounted onto the towing carriage. And then two force transducers were calibrated before installed on the slideway of the mechanism. The distance between two force transducers on the slideway was set as 1.6 m. Likewise, two supports were placed along the centerline of the ship hull with 1.6 m' separation and two supports are located symmetrically with respect to the center of gravity of the hull. Then the planar motion mechanism was mounted onto the carriage. The discrepancy between the mechanism's support plane and the carriage's back surface at eight points are controlled the same by eight screws, that ensures these two surface parallel planes. Last, the vertical position of the slideway was adjusted and two force transducers were connected to two supports on the hull.

2.3. Review of test conditions

In the model test, both static PMM tests (oblique towing) and dynamic PMM tests (pure sway, pure yaw, pure yaw with constant drift angles) are carried out. In this work, the authors mainly discuss three hydrodynamic derivatives X_{vv}, Y_v, N_v so only the static oblique towing tests are considered, the tests conditions are listed in Table 2.Where * indicates the conditions have been repeated 10 times for uncertainty analysis. And in tests 1–9, drift angles both to the port side and the starboard side are performed to yield the corrected data for symmetry with respect to the straight-ahead towing direction such that:

$$\chi_m = \frac{\chi^+ + \chi^-}{2} \tag{4}$$

where χ_m is the corrected data for any data variable ($\chi = X, Y, N$), and χ^+ or χ^- is the data χ respectively measured at positive or negative drift angle β. And all the measured variables are time averaged, cause the carriage speed oscillated during the towing tests. Besides, to analyze the effects of the advancing speed during PMM model tests on the hydrodynamic derivatives two advancing speed $U = 1.418m/s$ and $U = 0.709m/s$ are considered.

Table 2
Test conditions.

Test ID	Towing speed $U/(m/s)$	Drift angle $\beta/°$
1–9	1.418	0, ±2, ±4, ±6, ±8, ± 10*, ±12, ±16, ±20*
10–18	0.709	0,2,4,6,8, 10*, 12,16, 20*

3. Computational overview

3.1. Simulation approach and case setup

All the numerical calculations are based on the open-source CFD library OpenFOAM. The two-phase incompressible, isothermal immiscible fluids solver interDyMFoam, which use VOF (volume of fluid) – a phase-fraction based interface capturing approach, is used. The governing equation – unsteady Reynolds-average Navier-Stokes equation (URANS) is solved using the PIMPLE (coupled SIMPLE and PISO) algorithm to decouple pressure and velocity, and the multidimensional universal limiter for explicit solution (MULES) is used to solve the VOF equation. As for discretization schemes, the temporal term is discretized using second order backward scheme. The convective terms are discretized with the blended 75% linear and 25% second order upwind scheme, which is called LUST in OpenFOAM, and the diffusion terms are discretized with second order linear scheme.

The computational domain is $[-1L_{wl}: 3L_{wl}]$, $[-1.5L_{wl}: 1.5L_{wl}]$, $[-1L_{wl}: 0.5L_{wl}]$ in x, y, z directions respectively. The computational grids are generated in three steps. Firstly the OpenFOAM utility blockMesh is used to generate background grid. Secondly, refineMesh is applied to make a refinement of the free-surface region and near-hull region. Last, snappyHexMesh is used to generate the body-fitted grid and boundary layers. The thickness of the first grid layer is set as 0.0018 m to ensure the non-dimensional distance y^+ within the range 30–100, as is required by the standard wall function employed for the ship hull surface, for all the computational cases. The minimum grid size in z direction is $\Delta z = 0.001L_{wl}$ to capture waves generated by the ship, and numerical time step is $\Delta t = 0.001s$. Computational domain geometry and boundary conditions are illustrated in Fig. 3.

3.2. Computational conditions

Table 3 shows the computational cases conditions. A grid convergence and turbulence model study is performed in cases 1–10, for

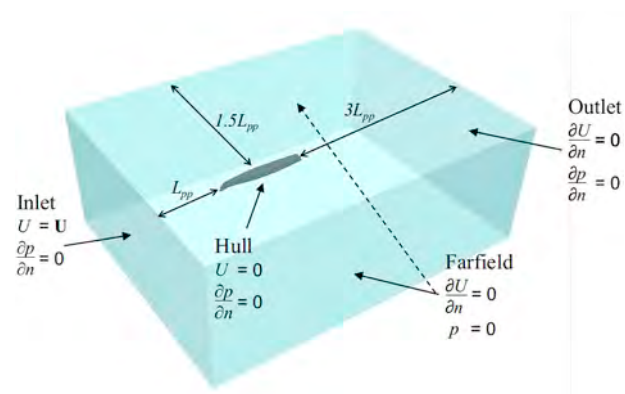

Fig. 3. Computational domain and boundary conditions.

Table 3
Computational cases conditions.

Case ID	Towing speed $U/(m/s)$	Drift angle $\beta/°$	Turbulence model	Mesh resolution
1–6	1.418	10	SST/DES	$C/M/F$
7–10		20	SST/DES	M/F
11–15		0,2,4,6,8	SST	M
16–17		12,16	DES	F
18–21	1.064	0,2.67, 5.33, 8	SST	M
22–25	0.709	0,4,8,12	SST	M
26–29	0.425	0,6.69, 13.46, 20.38	SST	M

which three grid resolutions (C, M, F short for coarse, medium and fine) and two turbulence models (SST, DES short for kOmegaSST and kOmegaSSTDES proposed in (Menter and Esch, 2001; Menter et al., 2003)) are used. The number of cells for C, M, F three grid levels are 3.5 million, 6 million and 11 million, with a refinement ratio of $\sqrt{2}$ in x, y, z three directions except for grid size at the free-surface region, where Δz is $0.001L_{wl}$ for all three grid resolutions. Fig. 4 illustrates the computational grids at the bow and stern region of the fine level grid, which shows that the wake region is refined to capture the flow separation and vortex shedding. And the results of different turbulence models, specifically kOmegaSST and kOmegaSSTDES, will demonstrate how turbulence model affects the simulation accuracy.

Simulation results of cases 1–17 and 22–25 will be compared with the experimental measurements for validation purpose and in cases 18–21 and 26–29, two more advancing speed are considered to figure out the relationship between advancing speed U and the hydrodynamic derivatives X_{vv}, Y_v, N_v.

3.3. Grid convergence and turbulence model study

As is mentioned in the previous setion, cases 1–10 are performed for grid convergence and turbulence model study. The results are compared with experimental measurements of the corresponding test conditions in Fig. 5. Figures in the first row demonstrate the results of cases 1–6 with drift angle $\beta = 10°$. As is illustrated, the numerical simulations of longitudinal force X, lateral force Y and moment along z axis N are basically within the 5% error bands of experimental measurements. And results predicted by kOmegaSSTDES model have bigger discrepancy with experimental measurements than that given by kOmegaSST model, especially when coarse and medium grids are used. Therefore we can conclude that, for the case with medium drift angle, in this case $\beta = 10°$, kOmegaSST turbulence model can capture the dominant flow features and is accurate enough. Besides, kOmegaSSTDES turbulence model needs higher-resolution grid to yield accurate results. The second row of Fig. 5 shows the results of cases 7–10 with drift angle $\beta = 20°$. As we can see, the numerical predictions of longitudinal force X and lateral force Y are all within the 5% error bands of experimental measurements. In contrast, the relative error of yaw moment N is slightly larger, particularly for kOmegaSST cases. But overall, the numerical results are in reasonable agreement with the experimental measurements and kOmegaSSTDES turbulence model can give more accurate results of forces and moment.

Based on the grid convergence and turbulence model study, the grid resolution and turbulence model used in other cases are determined. As is listed in Table 3, for cases 16–17 with high advancing speed and large drift angle ($\beta > 10°$), the calculations are performed using kOmegaSSTDES turbulence model and fine grid. And for cases 11–15, 18–29 with low advancing speed or small drift angle ($\beta \leq 10°$), the kOmegaSST turbulence model and medium grid are used. We have to mention that, the fine grid used in this work may not be fine enough for kOmegaSSTDES turbulence model. As is described in Stern et al. 2015, for static drift case the DES predictions improved when the grid points is refined beyond 84 million. But in this paper, to balance computing efficiency and accuracy, only 11 million cells are used for the fine grid.

4. Results and discussion

4.1. Validation of numerical prediction

Fig. 6 and Fig. 7 show calculated hydrodynamic forces X, Y and moment N in comparison with experimental measurements at two different advancing speed $U = 1.418m/s$ and $U = 0.709m/s$. In Fig. 6, *EFD* denotes the experimental data, as expressed in Eqn. (4), where χ^+ and χ^- respectively correspond to data measured at positive and negative drift angle, and *CFD* denotes numerical results given by cases 1–17. The 10% error bands are relative to the experimental data. Fig. 7 shows experimental measurements and numerical results obtained from tests 10–18 and cases 22–25. In Fig. 7, *EFD* denotes experimental data measured at positive drift angle and *CFD* denotes numerical predictions.

For longitudinal force X, the discrepancy between experimental data and calculated data is a little bit large, especially for cases with small drift angles $\beta < 10°$. As is illustrated, the measured longitudinal force oscillate a lot over drift angle, particularly for cases with lower advancing speed $U = 0.709m/s$ and the absolute value of longitudinal force is relatively small, so the mechanism vibration or towing speed instability may cause a large uncertainty for the measured data. Furthermore, the measurement range of the force sensor applied in the experiments is 500N and its accuracy is 0.3% of measurement range, which is 1.5N. However, the absolute error between CFD results and EFD measurements is about 1N. Generally speaking, the longitudinal force X is reasonably predicted. As for lateral force Y and moment along z axis N, the numerical predictions are basically within the 10% error bands of experimental measurements at both small and large drift angles. So it can be concluded that, the CFD solver, numerical methods and computational grids work well for this problem and the following study will be performed based on numerical predictions.

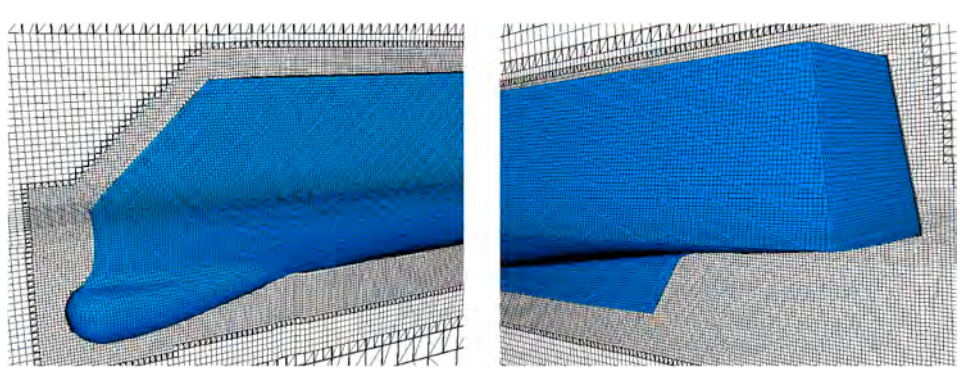

Fig. 4. Computational grids at bow (left) and stern (right) region.

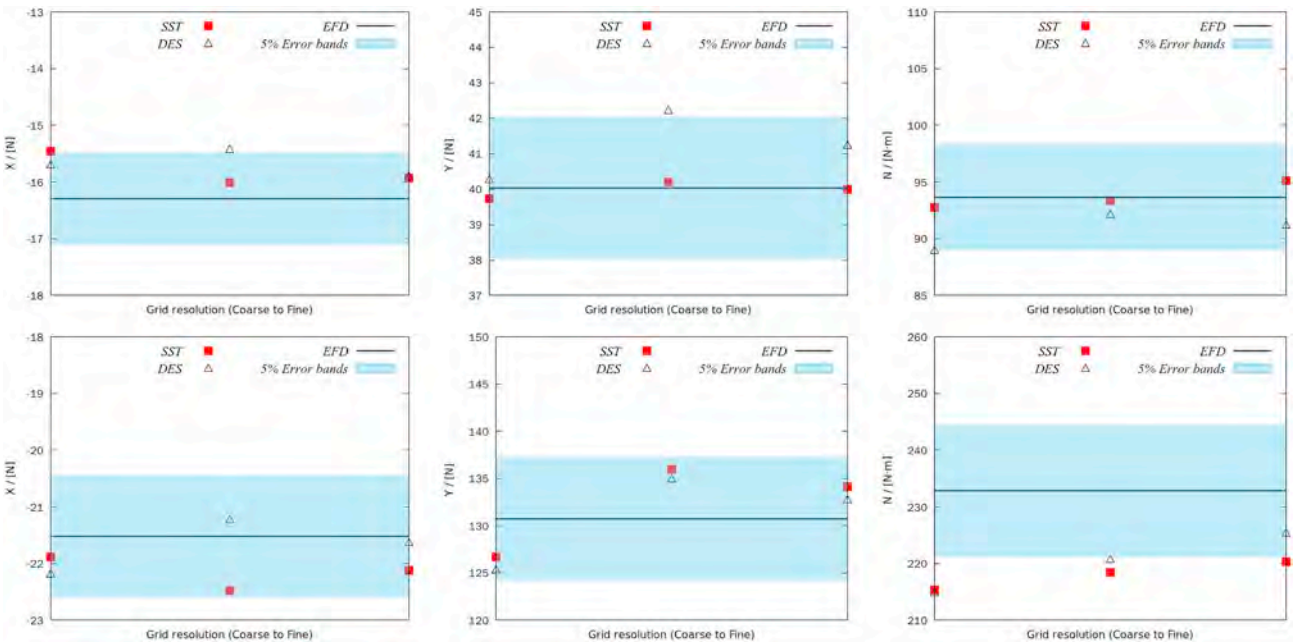

Fig. 5. Grid convergence and turbulence model study (X (left),Y (middle),N (right) results of cases 1–6 with drift angle $\beta = 10^{\circ}$ are in the first row and of cases 7–10 with drift angle $\beta = 20^{\circ}$ are in the second row.).

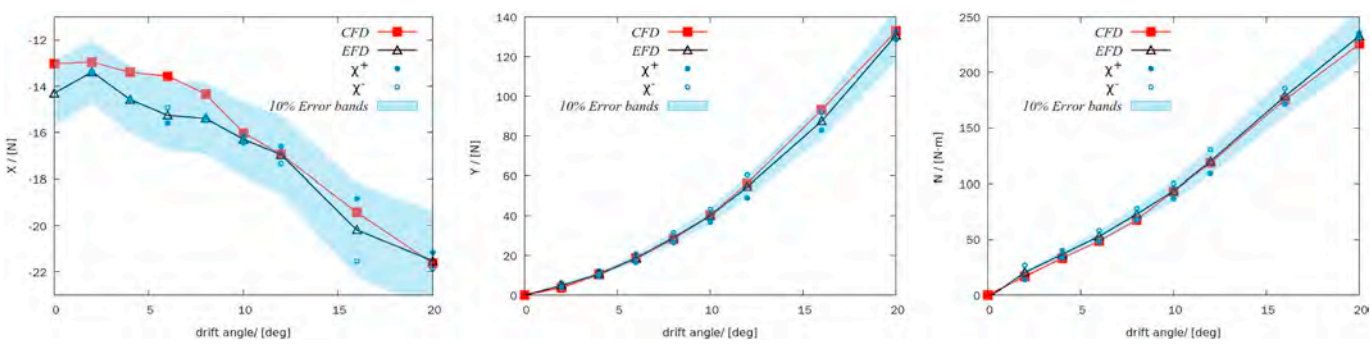

Fig. 6. Comparison between experimental measurements and numerical results of longitudinal force X (left), lateral force Y (middle) and moment along z axis N (right) of cases with advancing speed $U = 1.418m/s$.

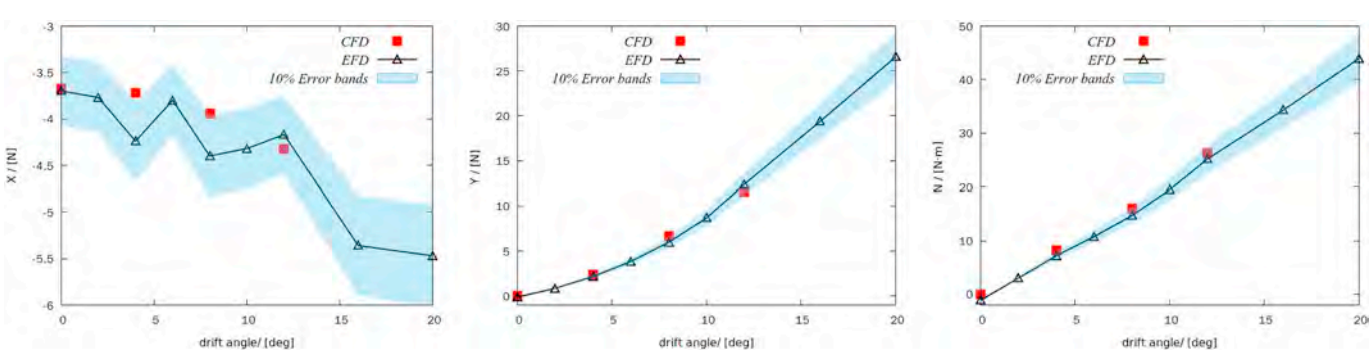

Fig. 7. Comparison between experimental measurements and numerical results of longitudinal force X (left), lateral force Y (middle) and moment along z axis N (right) of cases with advancing speed $U = 0.709m/s$.

4.2. Detail flow fields analysis

Fig. 8 illustrate the cross sections of flow field where the local velocity component along x axis U_x is smaller than 95% of advancing speed U of cases 1–17 with $U = 1.418m/s$. The cross sections are colored by vorticity magnitude; the ship hull is colored by dynamic pressure $p - \rho gh$ and the free surface is colored by z coordinate value.

As is shown in the figure, at small drift angle $\beta = 2^{\circ}$, there is one series of vortex generated by the sonar dome (hereafter called vortex **A**). As for medium drift angles $\beta = 4^{\circ}, 6^{\circ}, 8^{\circ}$, there are two sets of vortex – vortex **A** and vortex induced by the skeg (hereafter called vortex **B**), and with increasing of the drift angle, the vorticity strength substantially increased. Concerning big drift angles $\beta = 10^{\circ}, 12^{\circ}, 16^{\circ}, 20^{\circ}$, besides vortex **A** and vortex **B**, another series of vortex is generated by the ship hull (hereafter called vortex **C**). Vortex **C** is due to flow separation in the lateral direction and with increasing of drift angle the

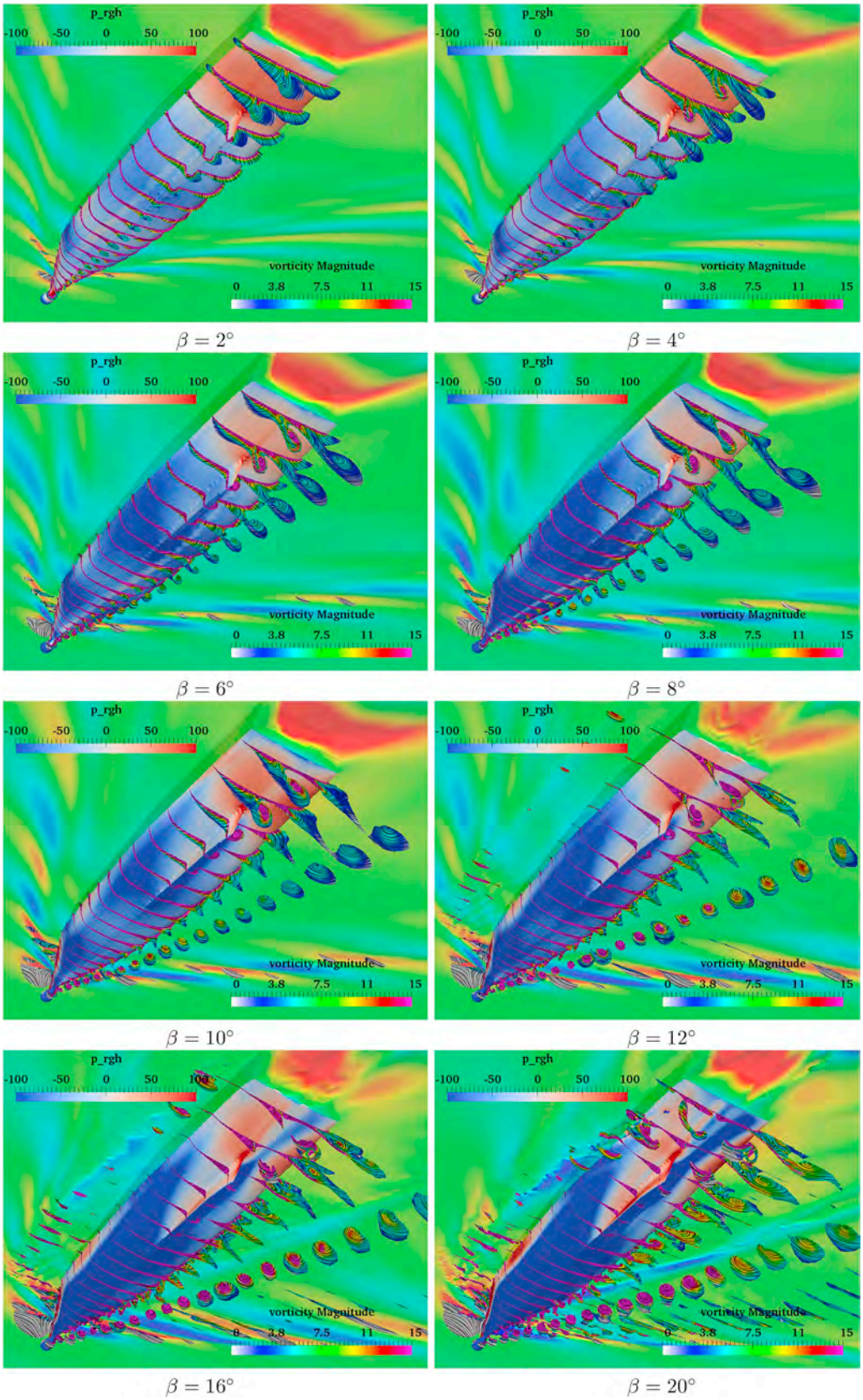

Fig. 8. Cross sections of flow field, colored by vorticity magnitude, along the ship hull of regions where the local velocity component along x axis U_x is smaller than 95% of advancing speed U.

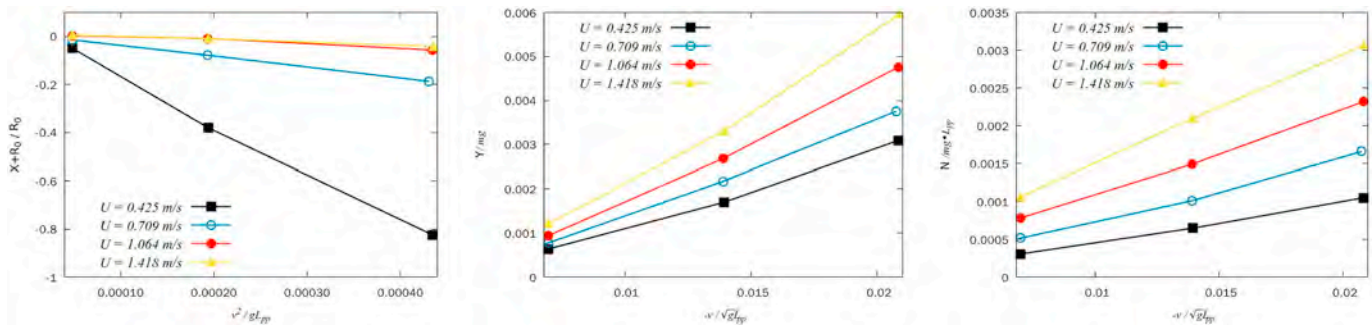

Fig. 9. Numerical results of longitudinal of force X minus resistance, lateral force Y and moment along z axis of four advancing speed.

Table 4
Hydrodynamic derivatives of the ONRT hull at four advancing speeds.

$U/(m/s)$	X'_{vv}	Y'_v	N'_v
0.425	−395.2	−0.137	−0.049
0.709	−88.2	−0.168	−0.077
1.064	−39.2	−0.211	−0.110
1.418	−23.9	−0.264	−0.148

separation point moves to the bow and central longitudinal section of the ship hull. As presented in literature (Xing et al., 2012; Jin et al., 2016; Abbas and Kornev, 2016), the kOmegaSST model smooth the flow features too much that is incapable to capture the unsteady vortex and flow separation accurately and the kOmegaSSTDES model may overestimate the vortex strength. As for the wave pattern we can also find the same phenomenon as (Abbas and Kornev, 2016) that, kOmegaSST model smooth the ship wave especially in the wake core region, but kOmegaSSTDES model can capture the unsteady wake effects.

5. Advancing speed effects on hydrodynamic derivatives

Fig. 9 illustrate the numerically predicted non-dimensional longitudinal force plus resistance $(X + R_0)/R_0$ with respect to square of lateral velocity v^2/gL_{wl}, non-dimensional lateral force Y/mg and yaw moment $N/(mg{\cdot}L_{wl})$ with respect to lateral velocity $v/\sqrt{gL_{wl}}$ of cases 11–14 and 18–29. As is described in Eqn. (5), $(X + R_0)/R_0$ has a linear correlation with v^2/gL_{wl} and Y/mg, $N/(mg{\cdot}L_{wl})$ have a linear correlation with $v/\sqrt{gL_{wl}}$. Consequently, the hydrodynamic derivatives or the slopes of all the curves can be yielded by a linear regression, which are listed in Table 4.

$$\begin{cases} \dfrac{X+R_0(U)}{R_0(U)} = \dfrac{X_{vv}(U)}{R_0(U)}\cdot gL_{wl}\cdot\dfrac{v^2}{gL_{wl}} = X'_{vv}\cdot\dfrac{v^2}{gL_{wl}} \\ \dfrac{Y}{mg} = \dfrac{Y_v(U)}{mg}\cdot\sqrt{gL_{wl}}\cdot\dfrac{v}{\sqrt{gL_{wl}}} = Y'_v\cdot\dfrac{v}{\sqrt{gL_{wl}}} \\ \dfrac{N}{mg\cdot L_{wl}} = \dfrac{N_v(U)}{mg\cdot L_{wl}}\cdot\sqrt{gL_{wl}}\cdot\dfrac{v}{\sqrt{gL_{wl}}} = N'_v\cdot\dfrac{v}{\sqrt{gL_{wl}}} \end{cases} \tag{5}$$

It is obvious that, the hydrodynamic derivatives of the ONRT ship hull vary a lot for different advancing speeds. Fig. 10 illustrates the relationship between dimensionless advancing speed $U' \equiv U/\sqrt{gL_{wl}}$ and hydrodynamic derivatives X'_{vv}, Y'_v, N'_v, where the scatters correspond to hydrodynamic derivatives yielded from Fig. 9 and the solid lines are fitted curves of hydrodynamic derivatives based on the least square method. For X'_{vv}, with the decrease of advancing speed the ship resistance $R_0(U)$ reduce to zero and then because of the asymmetry of ship bow and stern the magnitude of $X_{vv}(U = 0)$ is not zero, so the magnitude of X'_{vv} approaches infinite. Accordingly, we assume the hydrodynamic derivative X'_{vv} in the form of $X'_{vv} = 1/[U'^2{\cdot}(aU' + b)]$, where the coefficients a, b, determined via least square method, are $a \approx 7.1$, $b \approx 0.3$ respectively. Y'_v, N'_v vary linearly with the advancing speed that can be assumed in the form of $Y'_v = k_Y U' + c_Y$ and $N'_v = k_N U' + c_N$. Likewise, the coefficients k_Y, c_Y, k_N, c_N are determined by least square method that $k_Y \approx -0.906$, $c_Y \approx -0.08$, $k_N \approx -0.706$, $c_N \approx -0.006$. So we can concluded that, the hydrodynamic derivatives of the ONRT hull, specifically X'_{vv}, Y'_v, N'_v, vary greatly for different advancing speed and can be expressed as Eqn. (6).

$$\begin{cases} X'_{vv}(U') = \dfrac{1}{U'^2\cdot(7.1U'+0.3)} \\ Y'_v(U') = -0.906{\cdot}U' - 0.08 \\ N'_v(U') = -0.706{\cdot}U' - 0.006 \end{cases} \tag{6}$$

In order to figure out the effects of advancing speed on the vortex structures, Fig. 11 demonstrates the cross sections of flow field where the local velocity component along x axis U_x is smaller than 95% of advancing speed U. The results are from cases 29,25,21,14 with four different advancing speed respectively $U = 0.425m/s$, $0.709m/s$, $1.063m/s$, $1.418m/s$ and the same lateral velocity $v \approx -0.147m/s$. The same as Fig. 8, the cross sections are coloured by vorticity magnitude; the ship hull is coloured by dynamic pressure $p - \rho gh$ and the free surface is coloured by z coordinate value. Due to the difference on drift angle, vortex structures of the four cases varies considerably. For lower advancing speed cases $U = 0.425m/s$ and $U = 0.709m/s$, vortex **A,B,C** exist, and vortex **A** is away from the ship

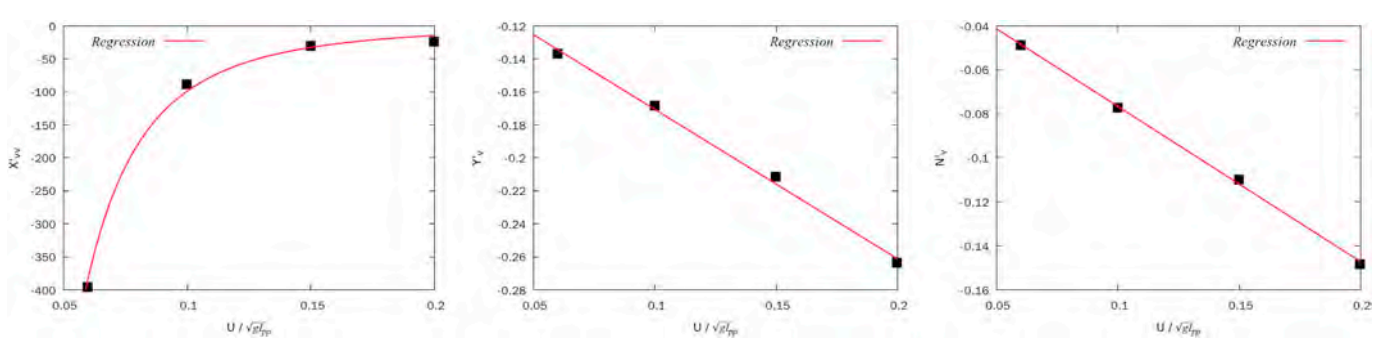

Fig. 10. Relationship between advancing speed and hydrodynamic derivatives.

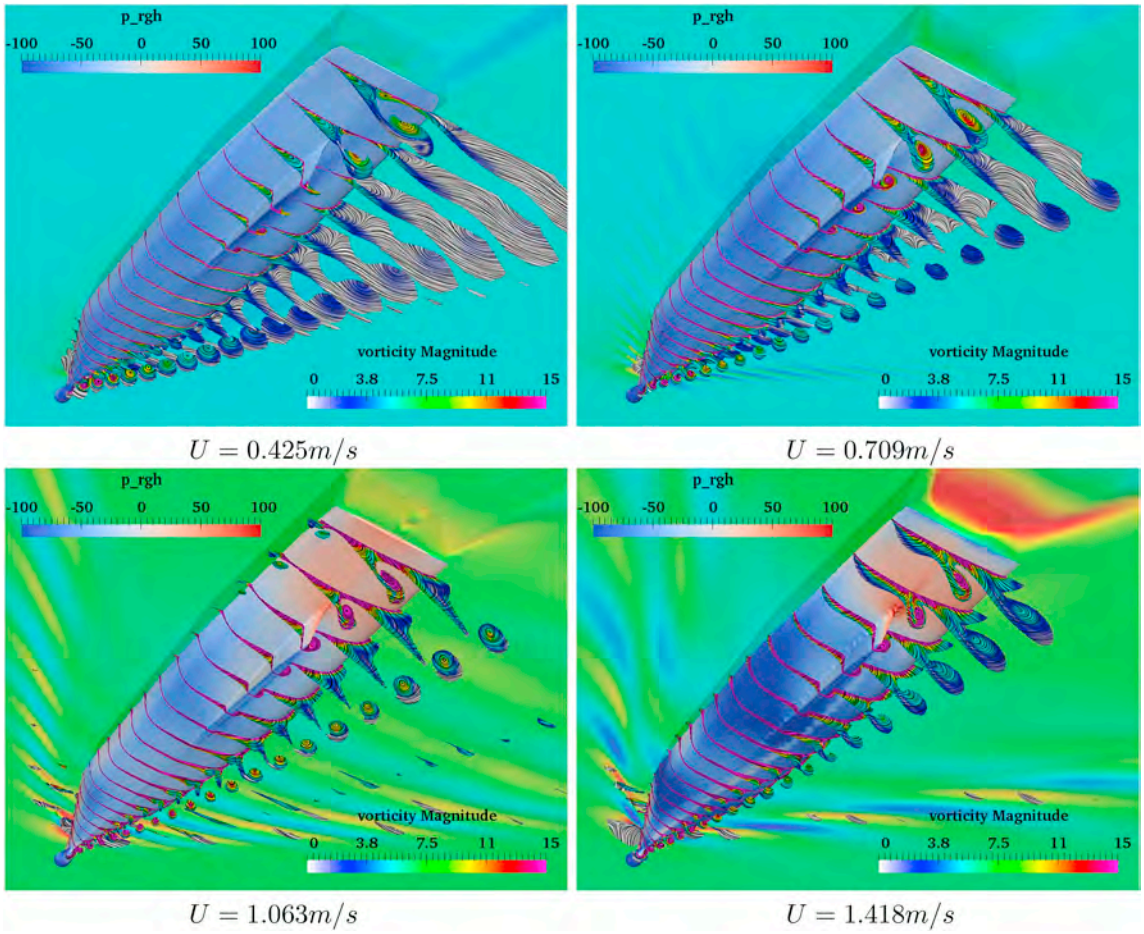

Fig. 11. Cross sections of flow field, coloured by vorticity magnitude, along the ship hull of regions where the local velocity component along x axis U_x is smaller than 95% of advancing speed U of cases with four advancing speed and the same lateral speed $v = -0.147m/s$.

hull at the stern region. For higher advancing speed cases $U = 1.063m/s$ and $U = 1.418m/s$ there are two sets of vortex – vortex **A,B** and for the case $U = 1.418m/s$ vortex **A** is still near the ship hull at the stern region that will influence the pressure distribution and lead to larger lateral force and yaw moment. With the increasing of the advancing speed U, the vortex strength increases and the wave elevation grows. All these factors are the basic reasons that yield different hydrodynamic forces and moment acting on the ship hull at different advancing speed.

6. Conclusions

In this paper experimental and numerical methods are used to perform oblique towing tests of the ONRT hull. First, the grid convergence and tubulence model study are performed for cases with medium drift angle $\beta = 10°$ and large drift angle $\beta = 20°$ and then based on these results, the grid resolution and turbulence model used for other cases are determined. For validation purpose, the numerical predictions of hydrodynamic forces and moment are compared with experimental measurements for cases with two advancing speed $U = 0.709m/s$ and $U = 1.418m/s$, and for most cases the numerical results of longitudinal force X, lateral force Y and moment along z axis N are within the 10% error bands of the experimental measurements. Thus the CFD solver, numerical methods and computing grids are proved accurate enough to simulate this problem. By analyzing the detail flow fields around the ship hull at different drift angles, we find that, when the ship is towing with low drift angle $\beta = 2°$, vortex **A** is generated by the sonar dome. And for the cases with medium drift angle $\beta = 4°, 6°, 8°$ vortex **B** is induced by the skeg. When the drift angle $\beta \geq 10°$, flow separation in the lateral direction happens, and vortex **C**, generated by the ship hull, becomes the dominant feature that affects the pressure distributions on the ship hull. Last, a numerical study of the advancing speed effects on hydrodynamic derivatives is performed. Oblique towing tests at four advancing speed $U = 0.425m/s, 0.709m/s, 1.063m/s, 1.418m/s$ are considered and three major hydrodynamic derivatives X_{vv}, Y_v, N_v at different advancing speed are studied. We find that, the relationship between X'_{vv} and $U' \equiv U/\sqrt{gL_{wl}}$ is $X'_{vv} = 1/(U'^2(aU' + b)$, where a, b can be determined via least square method. For the ONRT model, considered in this paper, $a \approx 7.1$, $b \approx 0.3$. And Y'_v, N'_v have a linear correlation with advancing speed that, $Y'_v = k_Y U' + c_Y$, $N'_v = k_N U' + c_N$. Based on the least square method, value of these coefficients are determined: $k_Y \approx -0.906$, $c_Y \approx -0.08$, $k_N \approx -0.706$, $c_N \approx -0.006$, where the intercept c_Y and c_N respectively represent the lateral force Y and moment along z axis exerted by the ship when it moves laterally without advancing speed.

To sum up, the relationship between non-dimensional hydrodynamic derivatives X'_{vv}, Y'_v, N'_v and advancing speed U' are obtained. But this relationship needs further application to the MMG model and show how much it influences the "Standards for Ship Maneuverability", such as tactical diameter, advance, overshoot angle et al., predicted by MMG model. On the other hand, all the studies performed in this paper are based on the ONRT ship hull, so further studies are needed to draw general conclusions for arbitrary type of ships.

References

Abbas, N., Kornev, N., 2016. Validation of hybrid URANS/LES methods for determination of forces and wake parameters of KVLCC2 tanker at manoeuvring conditions. Ship Technol. Res. 63 (2), 96–109.

Abkowitz, M.A., 1964. Lectures on ship hydrodynamics–steering and maneuverability. Report No. Hy-5. Hydro - og Aeordynamisk Laboratorium, Lyngby.

Broglia, R., Dubbioso, G., Durante, D., Di, M.A., 2015. Turning ability analysis of a fully appended twin screw vessel by CFD. part I: single rudder configuration. Ocean Eng. 105, 275–286.

Carrica, P.M., Ismail, F., Hyman, M., Bhushan, S., Stern, F., 2013. Turn and zigzag maneuvers of a surface combatant using a URANS approach with dynamic overset grids. J. Mar. Sci. Technol. 18 (2), 166–181.

He, S., Kellett, P., Yuan, Z., Incecik, A., Turan, O., Boulougouris, E., 2016. Manoeuvring prediction based on CFD generated derivatives. J. Hydrodyn. 28 (2), 284–292.

Jin, Y., Duffy, J., Chai, S., Chin, C., Bose, N., 2016. URANS study of scale effects on hydrodynamic manoeuvring coefficients of KVLCC2. Ocean Eng. 118, 93–106.

Liu, X., Nie, J., Xia, Z., Fan, S., et al., 2017. Investigation on the scale effect of maneuverability based on model tests and sea trials of a ship. In: The 27th International Ocean and Polar Engineering Conference. International Society of Offshore and Polar Engineers.

Menter, F., Esch, T., 2001. Elements of industrial heat transfer predictions. In: 16th Brazilian Congress of Mechanical Engineering, vol. 109 COBEM sn.

Menter, F., Kuntz, M., Langtry, R., 2003. Ten years of industrial experience with the SST turbulence model. Turbulence, heat and mass transfer 4 (1), 625–632.

Mofidi, A., Carrica, P.M., 2014. Simulations of zigzag maneuvers for a container ship with direct moving rudder and propeller. Comput. Fluids 96, 191–203.

Mucha, P., El Moctar, O., 2015. Revisiting mathematical models for manoeuvring prediction based on modified Taylor-series expansions. Ship Technol. Res. 62 (2), 81–96.

Ogawa, A., Koyama, T., Kijima, K., 1977. MMG report-I, on the mathematical model of ship manoeuvring. Bull Soc Naval Archit Jpn 575 (22–28).

Sadat-Hosseini, H., Wu, P., Carrica, P.M., Stern, F., 2014. CFD simulations of KVLCC2 maneuvering with different propeller modeling. In: Proceedings of SIMMAN2014 Workshop. Copenhagen, Denmark.

Shen, Z., Wan, D., Carrica, P.M., 2015. Dynamic overset grids in OpenFOAM with application to KCS self-propulsion and maneuvering. Ocean Eng. 108, 287–306.

Simonsen, C., Stern, F., 2014. SIMMAN 2014 workshop on verification and validation of ship maneuvering simulation methods. In: Draft Workshop Proceedings.

Stern, F., Wang, Z., Yang, J., Sadat-Hosseini, H., Mousaviraad, M., Bhushan, S., Diez, M., Sung-Hwan, Y., Wu, P., Yeon, S., et al., 2015. Recent progress in CFD for naval architecture and ocean engineering. J. Hydrodyn. 27 (1), 1–23.

Sung, Y., Park, S., 2015. Prediction of ship manoeuvring performance based on virtual captive model tests. Journal of the Society of Naval Architects of Korea 52 (5), 407–417.

Xing, T., Bhushan, S., Stern, F., 2012. Vortical and turbulent structures for KVLCC2 at drift angle 0, 12, and 30 degrees. Ocean Eng. 55, 23–43.

Yasukawa, H., Yoshimura, Y., 2015. Introduction of MMG standard method for ship maneuvering predictions. J. Mar. Sci. Technol. 20 (1), 37–52.